Investigations on the proton transport mechanism in potassium dihydrogenphosphate

1991 J. Phys.: Condens. Matter 3 5271

(http://iopscience.iop.org/0953-8984/3/28/003)

J. Phys.: Condens. Matter 3 (1991) 5271–5286. Printed in the UK

Investigations on the proton transport mechanism in potassium dihydrogenphosphate

Suresh Chandra and Ajay Kumar
Physics Department, Banaras Hindu University, Varanasi 221 005, India

Received 9 January 1991

Abstract. Transference number, mobility, differential thermal analysis, thermogravimetric analysis, infrared spectroscopy, and electrical conductivity as a function of temperature and humidity are reported on polycrystalline pellets and single crystals of potassium dihydrogenphosphate. The proton transport is anisotropic, the *c* axis being more favoured. The mobile species are H^+ and OH^-. The mobile species are the result of a threefold rotation of $H_2PO_4^-$ units about any of the axes of PO_4 tetrahedra giving O···H···H···O bonding, which rearranges as H···O···H···O. The H···O···H bridge is electrodissociated to give H^+ and OH^-. Finally, a P–O–P bond is formed between electrolysed $H_2PO_4^-$ groups.

1. Introduction

Potassium dihydrogenphosphate (KDP) belongs to the family of ferroelectric materials having structurally hydrogen-bonded protons. At room temperature, it remains in the paraelectric phase with tetragonal $I\bar{4}2d$ symmetry [1–4]. It consists of four molecules of KDP per unit cell with approximate cell dimensions $a = b \simeq 7.43$ Å and $c = 6.95$ Å. Each of the phosphate (PO_4) groups is tetrahedrally linked to four other PO_4 groups by hydrogen bonds, each having one proton towards the end of the bond. Thus, on average, every PO_4 group has two protons forming a network of $H_2PO_4^-$ ions attached to K^+ ions by ionic bonds. The hydrogen bonds associated with the phosphate group lie in a plane approximately perpendicular (~86°) to the *c* axis. KDP is a well established proton conductor in which the electrical conductivity has been attributed by many workers to be due to proton motion within the hydrogen-bond network.

Murphy [5] has suggested that, in ammonium dihydrogenphosphate (ADP), which has a structure similar to KDP, the proton migrates through the hydrogen-bond network by alternate interbond and intrabond jumps between $H_2PO_4^-$ units, i.e. L and D defect migration. According to O'Keeffe and Perrino [6], simultaneous thermally generated ions (ionization defects) and D and L defects are responsible for proton migration in KDP at higher temperatures, i.e. above the Curie temperature (122 K). On the basis of proton spin–lattice relaxation time measurements, Blinc and Pirš [7] have inferred that, in the paraelectric phase, fast interbond proton motion (ionization defects) is responsible for the dielectric relaxation of the KDP crystal, whereas slow rotation of $H_2PO_4^-$ units (forming D and L defects) around threefold axes of PO_4 tetrahedra dominates the DC electrical conductivity. The O–H···O bond has two potential minima separated by 0.4 Å, which cannot accommodate two protons simultaneously. Hence, the rotation of

0953-8984/91/285271 + 16 $03.50

$H_2PO_4^-$ units must have a cooperative process in which the rotation of one group induces the rotation of the other so that the hydrogen bond is vacant before the arrival of the new proton. Harris and Vella [8] considered D and L defects to be responsible for the proton transport in KDP. Sharon and Kalia [9] have proposed the synchronized rotation mechanism for the proton transport in KDP based on the rotation of $H_2PO_4^-$ units about the threefold axes of PO_4 tetrahedra [7]. Two types of rotation of PO_4 tetrahedra can be identified—one along the axis with no hydrogen and the other along the axis with the hydrogen bond. Sharon and Kalia [9] have argued that the formation of a D defect due to the rotation of $H_2PO_4^-$ units about an axis of PO_4 tetrahedra having no hydrogen is prohibited because the separation between the two potential minima in the O–H···O bond of KDP is only 0.4 Å, which cannot accommodate two protons at the same time and requires a high enthalpy. In the case of such rotation, an unstable situation like O···H···H···O between $H_2PO_4^-$ units will occur, which will be forced to revert back to its initial position by bidirectional axial rotation. Thus, it will not allow the proton to transfer from one $H_2PO_4^-$ unit to the other. Hence, they have considered the rotation of $H_2PO_4^-$ units only about the axes of PO_4 tetrahedra having hydrogen bonds resulting in a stable situation like O···H···O between $H_2PO_4^-$ units. As the rotation of $H_2PO_4^-$ units is of the bidirectional type, it is equally probable for the proton that has migrated to the other $H_2PO_4^-$ unit to come back to its initial position. This to-and-fro movement of the proton can be restricted to one direction by applying a DC electric field across the KDP sample.

The results of our experimental investigations, viz. coulometry, gas chromatography, infrared study, transient ionic current measurement and electrical conductivity measurement, are described in the following sections, which necessitate a 'new look' at the proton conduction mechanism in KDP.

2. Experimental details

The experimental investigations on KDP were carried out on polycrystalline pellets pressed at 10000 lb/cm^2 ($\sim 4.45 \times 10^8$ N m^{-2}). Some of the investigations were also performed on single crystals grown by slow evaporation of a saturated solution of KDP in triply distilled water in ambient atmosphere.

The ionic transference number of KDP was evaluated directly by two experiments: (i) Wagner's polarization measurement [10] and coulometry [11]. In Wagner's polarization method, one blocking and one non-blocking electrode are required. But in the case of our proton conducting material KDP, no suitable blocking or non-blocking electrode could be identified. Hence, this experiment was done by depositing a thick silver coating as blocking electrodes on both faces of KDP polycrystalline pellets using a vacuum evaporation technique. The result obtained, i.e. current versus time plot at fixed potential, has been taken as a guide to the Wagner's polarization behaviour. This method fails to separate out the contributions due to the anionic/cationic species in the total transference number.

Coulometry is a modified version of Tubandt's electrolysis method [12, 13]. In this experiment, the KDP sample (pellet/single crystal) was mounted on a double-arm electrolysis cell [11]. A constant current was passed through the sample. The volumes of the evolved gases at the cathode and the anode were measured as a function of time. The cathode gas (hydrogen) was gas chromatographically tested (Tracor Instruments, model 540).

The transient ionic current (TIC) measurement was carried out on a KDP pellet to identify the number of mobile ionic species and to evaluate their respective mobilities. Opposite faces of the sample pellet were thickly silver-coated to block the mobile ionic species. A fixed DC potential was applied across the sample to polarize it first. After some time the polarity was reversed. Current versus time was monitored. The experimental details have been reported elsewhere [14].

Infrared (IR) spectral studies on the original and the electrolysed KDP samples were performed to identify the electrodissociable groups and the corresponding mobile ionic species. Almost equal amounts of the original KDP material and the materials scraped from the anode and cathode sides of the electrolysed KDP pellet were separately dispersed in potassium bromide (KBr) in the ratio 1:100. Thin pellets were made and their IR spectra were recorded using a Perkin–Elmer IR spectrophotometer (model 783).

The thermal stability and the high-temperature phase transition in KDP were studied by differential thermal analysis (DTA) and thermogravimetric analysis (TGA) techniques in the temperature range 20–300 °C (293–573 K) using a Linseis DTA/TGA unit (type 2045). The heating rate was kept at 5 °C min^{-1}.

The electrical conductivity study was performed on KDP polycrystalline pellets and single crystals. Electrodes were made using silver paint. For measurements at selected spot frequencies of 100 Hz, 1 kHz and 10 kHz, a Wayne–Kerr high-precision bridge (model B905) was utilized. The bulk electrical conductivity was deduced from the complex impedance plot by measuring the real and imaginary parts of the impedance in the frequency range 1 Hz to 65 kHz using a Solartron Frequency Response Analyser (model 1250) with an Electrochemical Interface (model 1286) and HP computer (model 9122). The variation of conductivity with temperature was studied in the temperature range 294–490 K. From the conductivity versus temperature plot, the activation energy and the pre-exponential factor were evaluated. The humidity dependence of conductivity was also studied.

3. Results and discussion

3.1. Transference number

3.1.1. Wagner's polarization. Figure 1 shows Wagner's polarization curve (current versus time). From this curve, the total ionic transference number (t_i) was calculated using the equation [10]

$$t_i = 1 - i_e/i_T$$

where i_T and i_e are the initial current and the current after polarization respectively. The value of the ionic transference number evaluated was found to be 0.98, which implies that KDP is essentially an ionic conductor.

3.1.2. Coulometry. On passing a constant DC current through the KDP sample mounted on a double-arm electrolysis cell [11], gases were evolved at both the cathode and the anode. Figure 2 shows the plot of the evolved volume of gases as a function of time for KDP single crystals (along a/b axis and c axis) and polycrystalline pellets. The cathode gas was gas chromatographically tested and found to be hydrogen. The anode gas (supposedly oxygen) could not be tested owing to the lack of facilities.

The evolution of gases at both electrodes on application of a DC electric field across the KDP sample suggests the possible electrodissociation of the H···O···H bridges

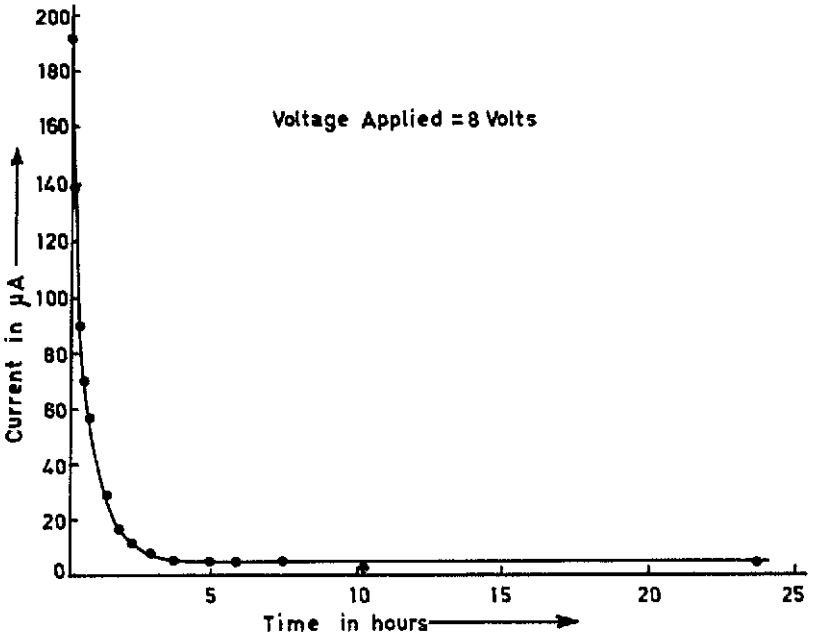

Figure 1. Wagner's polarization curve for KDP.

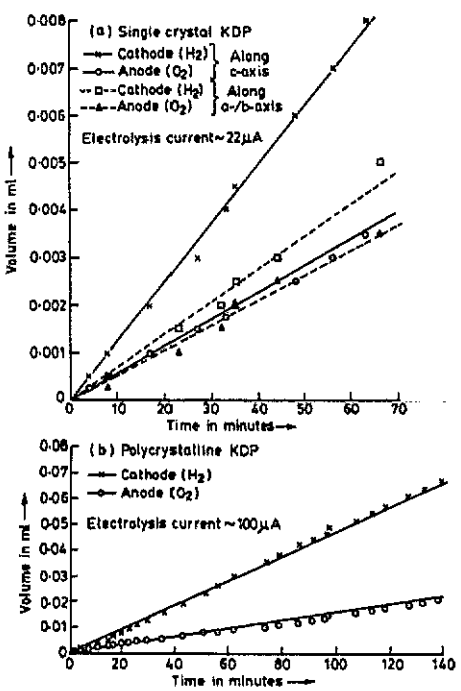

Figure 2. The volumes of the evolved gases in the coulometer as a function of time for (*a*) KDP single crystal along *a*/*b* axis (-----) and along *c* axis (——) and (*b*) KDP polycrystalline pellet.

Table 1. Transference number of KDP evaluated from coulometry assuming different mechanisms described in the text.

Material	Model/ mechanism	t_{H^+}	$t_{OH^-/H^{2-}}$	Total transference number, t_i
Polycrystalline pellet	I, III	0.64	0.49	1.13
	II	0.64	0.16	0.80
Single crystal *a*/*b* axis	I, III	0.48	0.68	1.16
	II	0.48	0.23	0.71
Single crystal *c* axis	I, III	0.76	0.67	1.43
	II	0.76	0.22	0.98

formed due to the rotation of $H_2PO_4^-$ units about the threefold axes of PO_4 tetrahedra generating H^+ and OH^-/O^{2-} as mobile ionic species. The following three possibilities have been considered:

Model I

$$2H_2O \rightarrow 4H^+ + 2O^{2-}$$

$$4H^+ + 4e^- \rightarrow 2H_2 \qquad \text{(at cathode)}$$

$$2O^{2-} \rightarrow O_2 + 4e^- \qquad \text{(at anode)}$$

Model II

$$4H_2O \rightarrow 4H^+ + 4OH^-$$

$$4H^+ + 4e^- \rightarrow 2H_2 \qquad \text{(at cathode)}$$

$$4OH^- \rightarrow 2H_2O + O_2 + 4e^- \qquad \text{(at anode)}$$

Model III

$$4H_2O \rightarrow 4H^+ + 4OH^-$$

$$4H^+ + 4e^- \rightarrow 2H_2 \qquad \text{(at cathode)}$$

$$4OH^- \xrightarrow[\text{back diffusion}]{2H_2O} O_2 + 4e^- \qquad \text{(at anode).}$$

Mechanism III differs from II in the sense that, for mechanism III, H_2O has been taken to diffuse back into the lattice after the charge-transfer reaction and only O_2 is liberated at the anode, whereas in mechanism II both H_2O and O_2 are liberated at the anode. Mechanisms I and III are similar as far as gas evolution is concerned and cannot be distinguished. The transference numbers calculated for H^+ and OH^-/O^{2-} on the basis of Faraday's laws of electrolysis from the observed volumes of evolved gases for all three models are given in table 1.

In the table, t_{H^+} and $t_{OH^-/O^{2-}}$ represent the respective transference numbers of H^+ and OH^-/O^{2-}. We expect the total transference number (t_i) to be less than 1 even if the total transference is due to ionic transport, since the actual volume of gases measured would be less than the evolved gases due to loss for various reasons (adsorption in

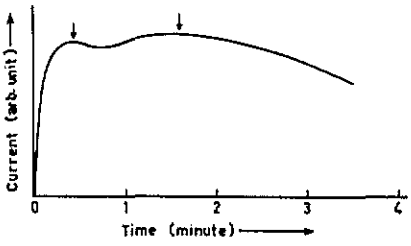

Figure 3. Current versus time plot of the transient ionic current measurement on KDP (see text).

mercury of the coulometer, possibility of small leakage, electrode reaction like $Hg + \frac{1}{2}O_2 \rightarrow HgO$, etc). Therefore, it seems that out of the proposed three models, model II is the most convincing, and thus H^+ and OH^- are the mobile species in KDP.

Another point that emerges from table 1 is that t_{H^+} is higher for the *c* axis as compared to the *a* (or *b*) axis and the value for the polycrystalline sample is intermediate between the two. This points out that the proton transport is anisotropic. The electrical conductivity measurements along *a* (or *b*) and *c* axes also confirm this (see section 3.5).

3.2. Mobility from transient ionic current (TIC) measurement

In this experiment, the sample was first polarized in a DC electric field and then the polarity was reversed. The current versus time was monitored. Two distinct peaks were obtained as shown in figure 3. From this, it is inferred that there are two mobile ionic species in KDP as suggested in the preceding section. By measuring the time (τ) taken for each peak, the mobility (μ) of each mobile ionic species was calculated using the equation

$$\mu = d^2/V\tau$$

where d is the thickness of the sample and V is the voltage applied to the sample. The results can be summarized as follows:

number of peaks	2
possible mobile species	H^+ and OH^-
mobility values	$\mu_{H^+} = 3.6 \times 10^{-5}$ cm^2 V^{-1} s^{-1}
	$\mu_{OH^-} = 9.3 \times 10^{-6}$ cm^2 V^{-1} s^{-1}

where μ_{H^+} and μ_{OH^-} are the mobilities of H^+ and OH^- ions, respectively.

Considering that equal charges are transported by cations (H^+) and anions (OH^-) under mechanism II discussed in section 3.1, the transference numbers of the mobile species can also be computed. The electrical conductivity σ_T (assuming no electron transport) and the conductivity contributions due to H^+ and OH^- (σ_{H^+} and σ_{OH^-}) can be written as

$$\sigma_T = ne(\mu_{H^+} + \mu_{OH^-}) \qquad \sigma_{H^+} = ne\mu_{H^+} \qquad \sigma_{OH^-} = ne\mu_{OH^-}.$$

From these we obtain

$$\sigma_{H^+}/\sigma_T = t_{H^+} = \mu_{H^+}/(\mu_{H^+} + \mu_{OH^-})$$

and

$$\sigma_{OH^-}/\sigma_T = t_{OH^-} = \mu_{OH^-}/(\mu_{H^+} + \mu_{OH^-}).$$

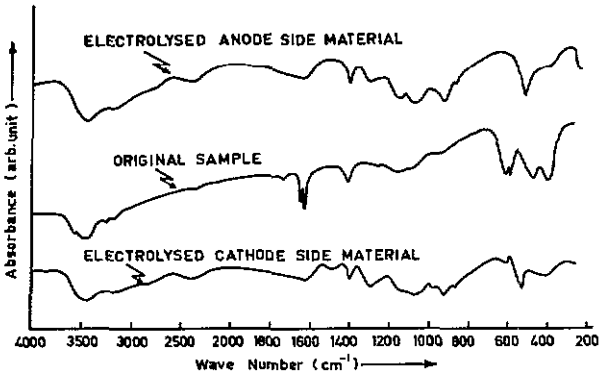

Figure 4. The IR absorption spectra of the original and electrolysed KDP.

The values of the transference numbers of H^+ and OH^- for polycrystalline KDP so calculated are given below along with the values obtained by coulometry (see section 3.1):

Transference number	From TIC	From coulometry
t_{H^+}	0.79	0.64
t_{OH^-}	0.21	0.16

It is evident from the above results that the values of the total ionic transference number obtained from the TIC and the coulometry experiments are in reasonably good agreement. The values obtained from the coulometry experiment are slightly less than those obtained from the TIC measurement. The two sets of values for transference number must be seen *vis-à-vis* their limitations. The present calculation from TIC banks heavily on the assumption that equal numbers of charge carriers are available for H^+ and OH^-, while the coulometry results (section 3.1) are likely to be low due to the unavoidable loss of evolved gases through adsorption, leakage, electrode reactions, etc.

3.3. The infrared (IR) spectral studies

The results presented above on coulometry and TIC measurements suggest that on the application of a DC electric field, H···O···H bridges in KDP formed due to the rotation of $H_2PO_4^-$ units become electrodissociated, yielding H^+ and OH^- ions as the mobile species. Therefore, the material obtained after the electrolysis must be different and show a different IR spectrum. The IR spectra of the original KDP material as well as the material scraped from the anode and cathode sides of the electrolysed KDP pellet were recorded as shown in figure 4. Salient changes in the IR spectra arising due to ion transport (resulting in the electrodissociation under DC field) are discussed below.

(i) Disappearance of the peaks at 3560, 3240, 1730, 1645 and 820 cm^{-1} after electrodissociation: These have been attributed to the electrolysis of the H···O···H bridges formed due to the rotation of $H_2PO_4^-$ units as shown in figure 5.

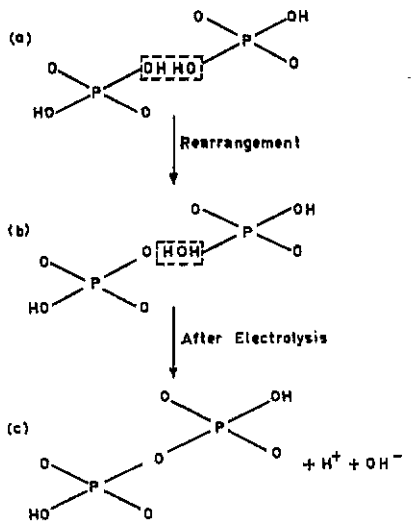

Figure 5. Schematic representation of the mechanism of proton transport in KDP.

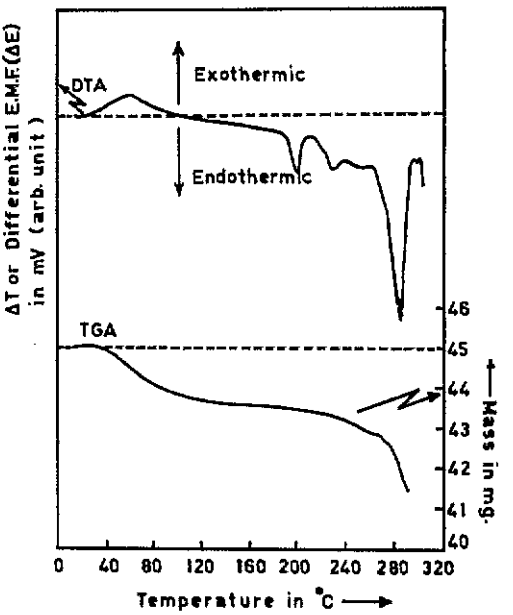

Figure 6. DTA and TGA curves for KDP single crystal in ambient atmosphere.

(ii) Appearance of a strong peak at 930 cm^{-1} superimposed over a broad 950 cm^{-1} peak: This has been assigned to the growth of the asymmetric P–O–P bond after electrodissociation as shown in figure 5 (discussed later).

(iii) Appearance of a new peak at 535 cm^{-1} after electrodissociation: This has also been assigned to the symmetric P–O–P bond formed by the process illustrated in figure 5.

(iv) Disappearance of the peak at 485 cm^{-1} after electrodissociation: It is reported by Blinc *et al* [15] that in KDP at higher temperatures the $H_2PO_4^-$ unit rotates and acquires such a configuration that intrabond proton tunnelling between the two equilibrium sites of the $H_2PO_4^-$ unit ceases and the corresponding peak (450 cm^{-1}) becomes weak. In the present case, it appears that a similar situation is created on application of the DC field through a process of $H_2PO_4^-$ group rotation and subsequent electrodissociation (as shown in figure 5) resulting in the disappearance of the 485 cm^{-1} peak.

On the basis of the above IR results together with those of the TIC measurement and coulometry, the ion transport mechanism can be suggested. A threefold rotation of $H_2PO_4^-$ units about any of the axes of PO_4 tetrahedra results in a situation like O···H···H···O (the D defect) as shown in figure 5(*a*). It rearranges itself in an unstable configuration as H···O···H···O illustrated in figure 5(*b*). This gets electrolysed/dissociated on application of the DC field, generating H^+ and OH^- as the mobile ionic species and a P–O–P bond results as shown in figure 5(*c*).

3.4. Thermal studies

The thermal stability and the high-temperature phase transition in KDP were studied by differential thermal analysis (DTA) and thermogravimetric analysis (TGA) techniques in

the temperature range 20–300 °C (293–573 K). For the DTA study alumina powder (Aldrich) was used as the reference material. Figure 6 shows the results of DTA and TGA of the KDP single crystals in an ambient atmosphere. There is a broad exothermic hump after ~29 °C in the DTA curve, which has been attributed to the release of surface adsorbed water. The onset of an endothermic peak at ~190 °C (peak position ~202 °C) in DTA corresponds to a structural transformation from tetragonal to monoclinic [15–17]. The temperature around 215 °C marks the beginning of yet another phase transition, which seems to be complex. There is no single peak but the phase transition seems to continue up to 240 °C in various steps as can be seen in figure 6. The two steps—the first at 221 °C and the second at 229 °C—have been attributed to the formation of the pyrophosphate and the triphosphate, respectively, as reported by Duval [18] as follows:

$$2KH_2PO_4 \rightarrow H_2O + K_2H_2P_2O_7 \qquad \text{(above 215 °C)}$$

and

$$KH_2PO_4 + K_2H_2P_2O_7 \rightarrow H_2O + K_3H_2P_3O_{10} \qquad \text{(above 229 °C)}.$$

The material melts in the temperature region 250–265 °C.

Similar to DTA results, the TGA result shown in figure 6 can also be understood. The initial decrease in mass starting at ~30 °C corresponds to desorption of the adsorbed water. The change in mass beyond 200 °C can be understood on the basis of the formation of pyrophosphate and triphosphate as given in the above chemical equations used for explaining DTA results. During the formation of pyro- and triphosphates, H_2O is released, resulting in the decrease of mass.

3.5. *Temperature dependence of electrical conductivity (σ)*

The results of the electrical conductivity study performed on KDP polycrystalline pellets (10000 lb cm^{-2}) and single crystals are discussed below.

3.5.1. σ versus $1/T$ at 100 Hz, 1 kHz and 10 kHz for KDP polycrystalline pellets. Figure 7 shows the temperature dependence of AC conductivity of KDP polycrystalline pellets measured at three fixed frequencies (100 Hz, 1 kHz and 10 kHz) by a Wayne–Kerr high-precision bridge (model B-905) in an ambient atmosphere as well as in vacuum. The results can be summarized as follows:

(i) The electrical conductivity in vacuum is very low ($\sigma_{vac} \sim 10^{-9}\ \Omega^{-1}\ cm^{-1}$). This indicates that KDP is not a very good proton conductor.

(ii) The electrical conductivity is humidity-dependent. The conductivity in air (humid) is higher (nearly 10^4 times at RH 62%) than the conductivity in vacuum. This indicates that the surface adsorbed water somehow triggers the proton conductivity by injecting H^+ ions.

(iii) As the temperature rises, the conductivity initially decreases (up to ~364 K) in air. This is an 'artifact' due to the desorption of surface adsorbed water. This effect is absent in σ versus $1/T$ measurements done in vacuum.

(iv) In vacuum, there is a change in the slope of the σ versus $1/T$ plot at ~370 K (region A). To check whether this variation in the slope is continuous or accompanied by a small discontinuity, the conductivity as a function of temperature was monitored at different heating rates as shown in figures 8 and 9. It is noted that, as the heating rate increases, a plateau in the temperature range 357–378 K becomes more obvious. Similar

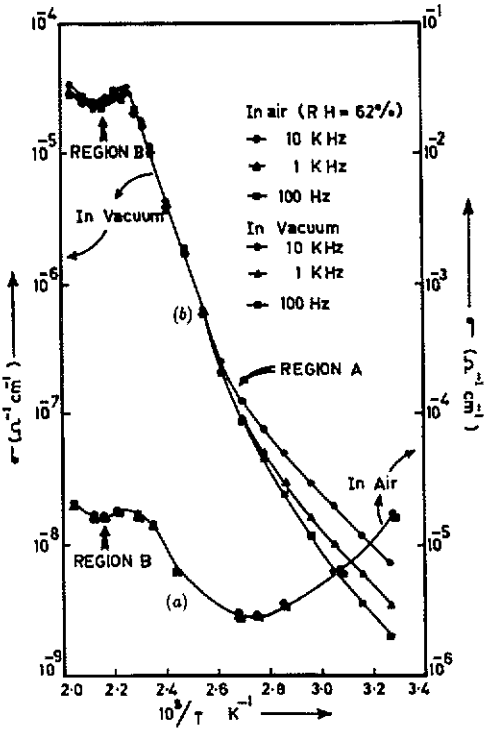

Figure 7. Temperature dependence of the AC electrical conductivity of KDP polycrystalline pellet at three frequencies in (*a*) air and (*b*) vacuum at a heating rate of 0.5 °C min^{-1}.

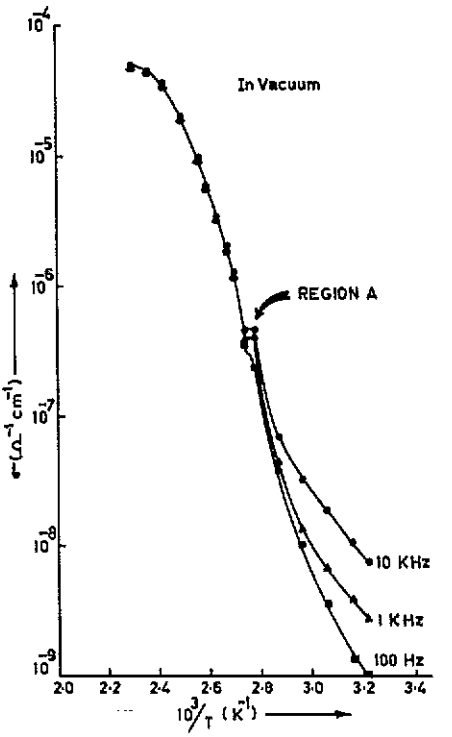

Figure 8. Temperature dependence of the AC electrical conductivity at three frequencies for KDP polycrystalline pellet in vacuum at a heating rate of 0.65 °C min^{-1}.

anomalous behaviour is reported by Pereverzeva *et al* [19] and Poplavko *et al* [20] in dielectric constant and thermal expansion coefficient measurements, respectively, along the tetragonal *a* axis of a KDP single crystal.

(v) At ~467 K (region B), a dip is observed in σ measurements done in both humid air and vacuum (see figure 7). This is attributed to the structural change from tetragonal to monoclinic as discussed in the thermal studies (section 3.4).

3.5.2. σ versus $1/T$ at 100 Hz, 1 kHz and 10 kHz for KDP single crystals. The temperature dependence of AC conductivity of KDP single crystals measured along *a* (or *b*) and *c* axes at different frequencies (100 Hz, 1 kHz and 10 kHz) by Wayne–Kerr high-precision bridge (model B-905) is shown in figures 10 and 11. The results can be summarized as given below:

(i) As in the case of the pellet, the conductivity initially decreases with temperature in air (humid) but not in vacuum, where it follows nearly Arrhenius-type behaviour. The same explanation can be offered for single crystals and pellets, that the initial decrease in conductivity in humid air is an 'artifact' due to surface adsorbed water.

(ii) The conductivity in vacuum is less than the conductivity in air (humid), a result similar to that for the polycrystalline pellet.

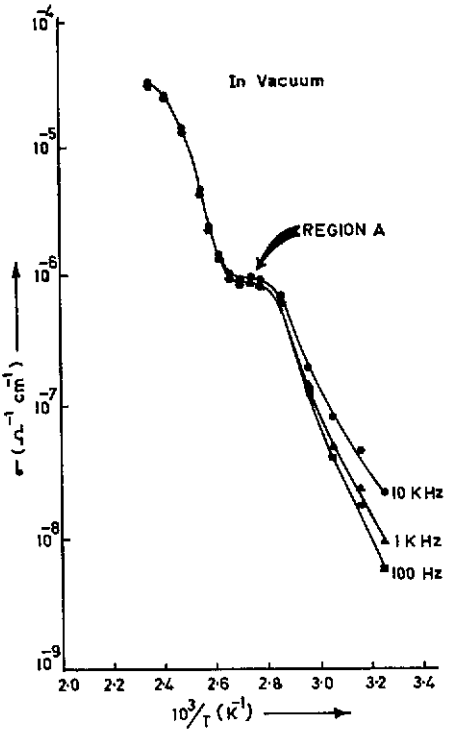

Figure 9. Temperature dependence of the AC electrical conductivity at three frequencies for KDP polycrystalline pellet in vacuum at a heating rate of 1.0 °C min^{-1}.

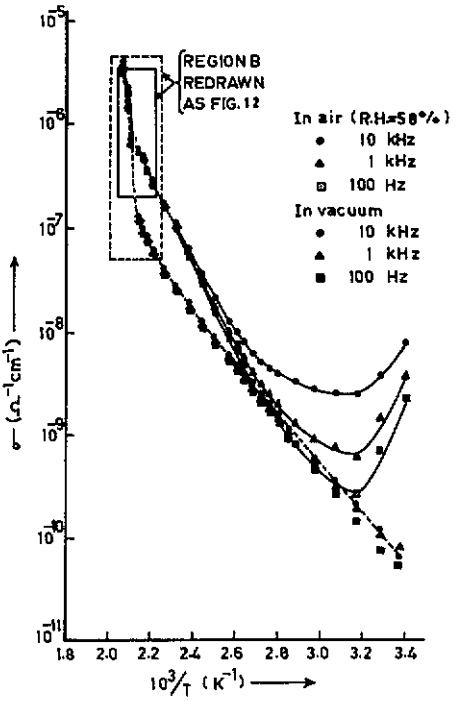

Figure 10. Temperature dependence of the AC electrical conductivity of KDP single crystal along a/b axis in air and vacuum.

(iii) In vacuum the electrical conductivity of a KDP single crystal is anisotropic. The values of $\sigma_c > \sigma_{a,b}$, as shown in figures 10 and 11.

(iv) It may be noted that we have observed a conductivity hump at $T \sim 377$ K in the σ versus $1/T$ plot on KDP pellets (region A in figures 8 and 9). The question is to examine whether this hump is due to changes in $\sigma_{a,b}$ or σ_c at this temperature. A close examination of figures 10 and 11 shows that it is σ_c which shows a change in conductivity at $T \sim 377$K (and not $\sigma_{a,b}$). This must in some way be related to the rotation of the $H_2PO_4^-$ group. Slater [1] has argued that there are six possible arrangements of the hydrogens about the oxygens of a PO_4 group. Four arrangements are similar but two are energetically different. In these two arrangements, the two hydrogens attached to a PO_4 group are either both on the 'upper' side of the group (i.e. the side along the positive c direction) or both on the 'lower' side (i.e. the side along the negative c direction); whereas in the other four arrangements, one hydrogen is on the 'upper' side and the other on the 'lower' side. Each arrangement makes the $H_2PO_4^-$ group an electrical dipole. The dipole in the arrangement having the hydrogens 'up' points along the positive c direction and that in the arrangement having the hydrogens 'down' points along the negative c direction. On the other hand, in the other four arrangements having one hydrogen 'up' and one 'down', the dipole points in a plane perpendicular to the c direction. Since the c axis is the preferred axis in the crystal, the two orientations of the dipole along the $\pm c$ axis can

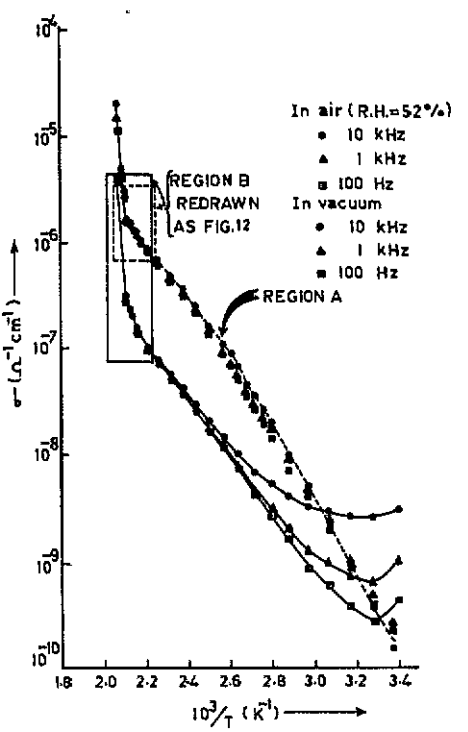

Figure 11. Temperature dependence of the AC electrical conductivity of KDP single crystal along c axis in air and vacuum.

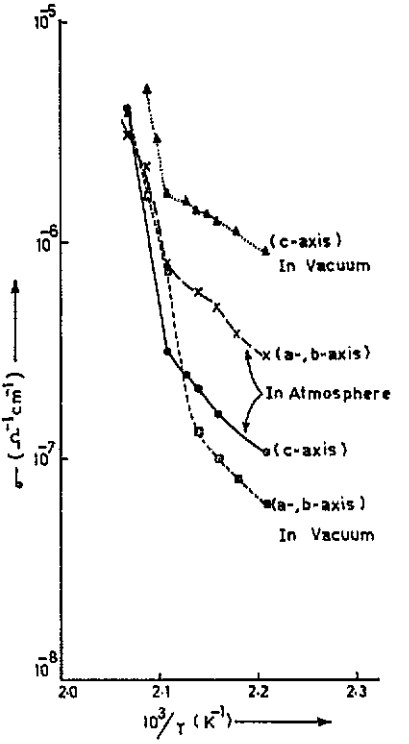

Figure 12. Variation of the AC electrical conductivity (at 10 kHz) of KDP single crystal in the temperature range 452–483 K.

have different energy from those perpendicular to the c axis. The dielectric behaviour of the crystal shows that the orientations along the $\pm c$ axis must have a lower energy than those at right angles. Thus, there is a tendency for spontaneous polarization along these directions. The state of lowest energy will come when each dipole is oriented either along the positive c or negative c axis. Therefore, we expect that a proton rotation of the $H_2PO_4^-$ group would give rise to a dielectric anomaly along the a or b axis and would facilitate proton transport along the c axis. The dielectric anomaly expected from the above arguments has been observed by Pereverzeva *et al* [19]. The conductivity anomaly can be seen in figure 11. At this temperature $T \sim 377$ K the structural change is not as apparent. The tetragonal symmetry is maintained and a possible change in the space group takes place from $I\bar{4}2d$ to $I4_1md$ [17].

(v) Now, we direct our attention to the region B in σ versus $1/T$ plot shown in figures 10 and 11. In the temperature range 463–474 K a plateau in the σ versus $1/T$ plots of single crystals is observed. This is shown on an enlarged scale in figure 12. After the plateau due to pretransition behaviour, σ suddenly rises. At $T \sim 467$ K, KDP is known to undergo a phase transition from tetragonal to monoclinic [17]. During the transition, a large stress is built up in the crystals, which results in the cracking of the crystals, and the transparent colourless KDP single crystals became opaque and milky.

3.5.3. σ versus $1/T$ from complex impedance plot. The bulk electrical conductivity of a polycrystalline pellet of KDP was deduced from the complex impedance plots in the

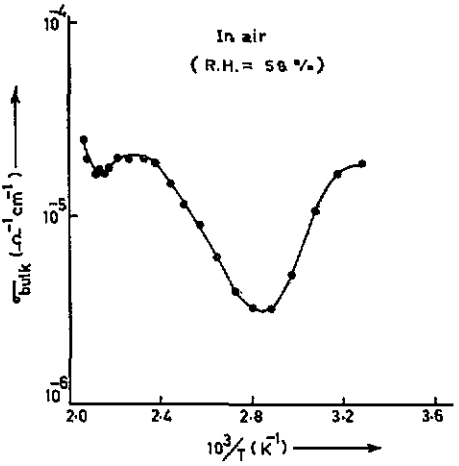

Figure 13. Temperature dependence of the bulk electrical conductivity of KDP polycrystalline pellet derived from the complex impedance plots.

temperature range 299–501 K. Figure 13 shows the temperature dependence of the bulk conductivity of a KDP pellet in ambient atmosphere (humid). Qualitatively, the results are similar to those discussed earlier in this section for a KDP polycrystalline pellet at fixed frequencies.

Complex impedance plots for KDP single crystals could not be obtained because of their high resistance mismatching the input impedance of the Solartron assembly.

3.5.4. Activation energy. The σ versus $1/T$ plots discussed earlier show that proton transport is a thermally activated process. However, we note that the entire temperature dependence cannot be represented by one single slope because of the complex phase transition behaviour. Broadly, the σ versus $1/T$ plots can be divided into the following two temperature regions:

region I	from 305 to 348 K
region II	from 380 to 435 K.

In these two regions, the plots can be represented by the equation

$$\sigma = \sigma_0 \exp(-E_a/kT)$$

with different values of pre-exponential factor σ_0 and activation energy E_a. We have not considered temperatures below 305 K because in many cases it gives rise to an 'artifact' due to surface adsorbed water. The activation energy E_a and the pre-exponential factor σ_0 for each case (given earlier in figures 7, 10, 11 and 13) are given in table 2.

The disturbing result is the high values of σ_0 ($\sim 10^8\ \Omega^{-1}\ \text{cm}^{-1}$) and E_a (~ 1.15 eV) for the polycrystalline sample in vacuum in the temperature range 380–435 K. There is an obvious pre-exponential anomaly. In the same temperature range, the ambient atmosphere data show no pre-exponential anomaly and give $\sigma_0 \sim 10^{-1}\ \Omega^{-1}\ \text{cm}^{-1}$, $E_a \sim 0.40$ eV. Similarly, no predominant pre-exponential anomaly is seen for single-crystal data in vacuum. The pre-exponential anomaly for the polycrystalline data in vacuum has to be looked into within the framework of the analysis given by Nowick and Lee [21]. In the present case, the high value of σ_0 may be related to an additional enthalpy term involving association or trapping. We have already recognized the importance of

Table 2. Pre-exponential factor and activation energy of KDP in different temperature regions.

Temp. range (K)	Material	Medium	Type of measurement	Conductivity, σ^a (Ω^{-1} cm^{-1})
380–435	Polycrystalline	Air (RH = 58%)	Complex impedance plot	$\sigma = 7.48 \times 10^{-1} \exp(-0.38/kT)$
380–435	Polycrystalline	Air (RH = 62%)	10 kHz	$\sigma = 6.20 \times 10^{-1} \exp(-0.40/kT)$
380–435	Single crystal a/b axis	Air (RH = 58%)	10 kHz	$\sigma = 22.20 \exp(-0.71/kT)$
380–435	Single crystal c axis	Air (RH = 52%)	10 kHz	$\sigma = 1.55 \times 10^{-2} \exp(-0.47/kT)$
380–435	Polycrystalline	Vacuum	10 kHz	$\sigma = 4.34 \times 10^{8} \exp(-1.15/kT)$
380–435	Single crystal a/b axis	Vacuum	10 kHz	$\sigma = 4.04 \times 10^{-2} \exp(-0.53/kT)$
380–435	Single crystal c axis	Vacuum	10 kHz	$\sigma = 4.26 \times 10^{-1} \exp(-0.5/kT)$
305–348	Polycrystalline	Air	10 kHz	Could not be evaluated due to adsorbed water effects
305–348	Polycrystalline	Vacuum	10 kHz	$\sigma = 1.62 \times 10^{-2} \exp(-0.38/kT)$
305–348	Single crystal a/b axis	Vacuum	10 kHz	$\sigma = 5.57 \times 10^{-3} \exp(-0.47/kT)$
305–348	Single crystal c axis	Vacuum	10 kHz	$\sigma = 4.24 \times 10^{2} \exp(-0.73/kT)$

[a] Conductivity given by $\sigma = \sigma_0 \exp(-E_a/kT)$.

surface adsorbed water in triggering proton transport (which in the case of polycrystalline samples would also include adsorbed water in the intergrain space). When the sample is put in vacuum and the temperature is increased, the intergrain adsorbed water may be pumped out, offering intergrain traps for transporting protons. Therefore, σ_0 and E_a evaluated from the polycrystalline data have to be looked at with caution.

3.6. Humidity dependence of electrical conductivity

The complex impedance plots for KDP polycrystalline pellets at different relative humidity levels (10% to 90%) are given in figure 14. The values of σ evaluated from these plots along with the σ values at 10 kHz for different relative humidity (RH) are shown in figure 15. The high RH was obtained by putting water inside the conductivity measurement chamber. Subsequently, water was removed and desiccant was put in to reduce the humidity. As the RH increases, the bulk resistance of KDP polycrystalline pellets decreases because of the increase in surface adsorbed water, which enhances the proton conductivity by injecting H^+ ions. The increase in conductivity is faster at RH > 70% because of surface dissolution and high adsorption of water. This is apparent in the complex impedance plot at higher humidity levels in which a complex loop starts to appear, indicating the onset of a dissolution reaction.

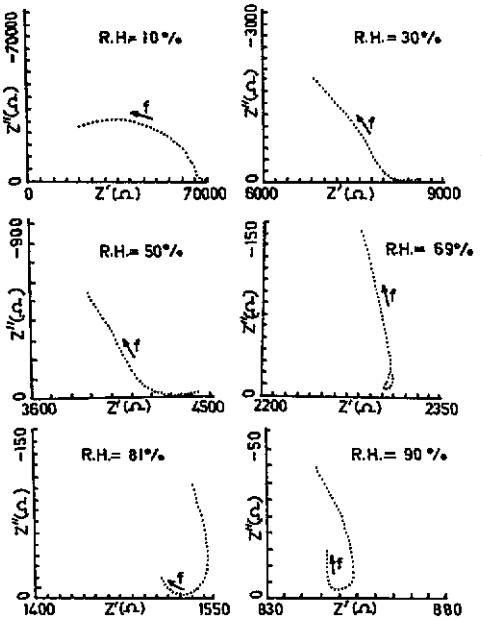

Figure 14. Complex impedance plots of KDP polycrystalline pellet at different humidity levels.

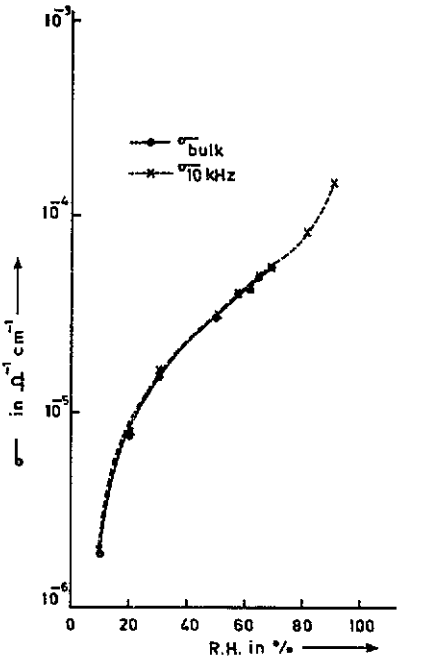

Figure 15. Variation of the electrical conductivity of KDP polycrystalline pellet as a function of humidity level.

4. Conclusions

On the basis of the results obtained from the electrical, thermal and spectroscopic investigations on KDP polycrystalline pellets/single crystals, the following conclusions have been drawn. The total ionic transference number as evaluated from Wagner's polarization method and coulometry shows that KDP is essentially an ionic conductor. The two peaks observed during TIC measurement, the evolution of gases at the cathode and anode during coulometry, the gas chromatography of cathode gas, and the comparative IR spectral studies of the original and electrolysed KDP material have led us to suggest a proton transport mechanism in KDP. A threefold rotation of $H_2PO_4^-$ units about any of the axes of the PO_4 tetrahedra leads to a situation like $O\cdots H\cdots H\cdots O$. This rearranges itself like $H\cdots O\cdots H\cdots O$, forming an $H\cdots O\cdots H$ bridge. This $H\cdots O\cdots H$ bridge becomes electrodissociated on application of a DC electric field, producing H^+ and OH^- ions as mobile charge species. Ultimately, a P–O–P bond is formed between electrolysed $H_2PO_4^-$ groups.

The electrical conductivity measurements along different crystallographic axes of KDP single crystals show the anisotropy in conductivity. The temperature variation of conductivity shows anomalous behaviour in the polycrystalline pellet and single crystal along the *c* axis in the temperature range 357–378 K because of $H_2PO_4^-$ group rotation forming an electrical dipole. It also shows conductivity variation corresponding to the structural phase transition at ~467 K observed in thermal studies. The variation of electrical conductivity with humidity level shows an increase in conductivity with rise in humidity level because of proton injection by the surface adsorbed water.

Acknowledgments

We thank the Department of Non-Conventional Energy Sources (Govt of India) for financial assistance. One of us (AK) thanks CSIR (India) for the award of a Senior Research Fellowship. Thanks are due to Dr S P Singh and Dr K D Pandey (Department of Botany, BHU) for helping in gas chromatographic studies.

References

[1] Slater J C 1941 *J. Chem. Phys.* **9** 16
[2] de Quervain M 1944 *Helv. Phys. Acta* **17** 509
[3] Ubbelohde A R and Woodward I 1947 *Proc. R. Soc.* A **188** 358
[4] Frazer B C and Pepinsky R 1953 *Acta Crystallogr.* **6** 273
[5] Murphy E J 1964 *J. Appl. Phys.* **35** 2609
[6] O'Keeffe M and Perrino C T 1967 *J. Phys. Chem. Solids* **28** 211
[7] Blinc R and Pirš J 1971 *J. Chem. Phys.* **54** 1535
[8] Harris L B and Vella G T 1973 *J. Chem. Phys.* **58** 4550
[9] Sharon M and Kalia A K 1977 *J. Solid State Chem.* **21** 171
[10] Wagner J B and Wagner C 1957 *J. Chem. Phys.* **26** 1597
[11] Chandra S, Singh N and Singh B 1986 *Solid State Commun.* **57** 519
[12] Tubandt C 1920 *Z. Anorg. Allg. Chem.* **110** 234
[13] Tubandt C 1920 *Z. Anorg. Allg. Chem.* **115** 105
[14] Chandra S, Tolpadi S K and Hashmi S A 1988 *Solid State Ionics* **28–30** 651
[15] Blinc R, Dimic V, Kolar D, Lahajnar G, Stepišnik J, Žumer S, Vene N and Hadzi D 1968 *J. Chem. Phys.* **49** 4996
[16] Grindberg J, Levin S, Pelah I and Wiener E 1967 *Solid State Commun.* **5** 863
[17] Itoh K, Matsubayashi T, Nakamura E and Motegi H 1975 *J. Phys. Soc. Japan* **39** 843
[18] Duval C 1963 *Inorganic Thermogravimetric Analysis* (New York: Elsevier) p 258
[19] Pereverzeva L P, Pogsskaya N Z, Poplavko Y M, Pakhamov V I, Rez I S and Sil'nitskaya G B 1972 *Sov. Phys.–Solid State* **13** 2690
[20] Poplavko Y M, Rez I S, Gorbokon N V and Dimarova E N 1972 *Sov. Phys.–Crystallogr.* **17** 595
[21] Nowick A S and Lee W 1989 *Superionic Solids and Solid Electrolytes—Recent Trends* ed A L Laskar and S Chandra (New York: Academic) p 381